9214–9231 *Nucleic Acids Research, 2015, Vol. 43, No. 19* *Published online 3 August 2015*
doi: 10.1093/nar/gkv782

Mediator independently orchestrates multiple steps of preinitiation complex assembly *in vivo*

Fanny Eyboulet[1], Sandra Wydau-Dematteis[1], Thomas Eychenne[1], Olivier Alibert[2], Helen Neil[1], Claire Boschiero[1], Marie-Claire Nevers[3], Hervé Volland[3], David Cornu[4], Virginie Redeker[4], Michel Werner[1] and Julie Soutourina[1,*]

[1]Institute for Integrative Biology of the Cell (I2BC), Institut de Biologie et de Technologies de Saclay (iBiTec-S), CEA, CNRS, Université Paris Sud, F-91191 Gif-sur-Yvette cedex, France, [2]CEA, iRCM, LEFG, Genopole G2, F-91057 Evry cedex, France, [3]CEA, iBiTec-S, Service de Pharmacologie et d'Immunoanalyse, F-91191 Gif sur Yvette cedex, France and [4]CNRS, Centre de Recherche de Gif, SICaPS, F-91198 Gif-sur-Yvette cedex, France

Received January 21, 2015; Revised July 17, 2015; Accepted July 21, 2015

ABSTRACT

Mediator is a large multiprotein complex conserved in all eukaryotes, which has a crucial coregulator function in transcription by RNA polymerase II (Pol II). However, the molecular mechanisms of its action *in vivo* remain to be understood. Med17 is an essential and central component of the Mediator head module. In this work, we utilised our large collection of conditional temperature-sensitive *med17* mutants to investigate Mediator's role in coordinating preinitiation complex (PIC) formation *in vivo* at the genome level after a transfer to a non-permissive temperature for 45 minutes. The effect of a yeast mutation proposed to be equivalent to the human Med17-L371P responsible for infantile cerebral atrophy was also analyzed. The ChIP-seq results demonstrate that *med17* mutations differentially affected the global presence of several PIC components including Mediator, TBP, TFIIH modules and Pol II. Our data show that Mediator stabilizes TFIIK kinase and TFIIH core modules independently, suggesting that the recruitment or the stability of TFIIH modules is regulated independently on yeast genome. We demonstrate that Mediator selectively contributes to TBP recruitment or stabilization to chromatin. This study provides an extensive genome-wide view of Mediator's role in PIC formation, suggesting that Mediator coordinates multiple steps of a PIC assembly pathway.

INTRODUCTION

In eukaryotes, the synthesis of mRNAs and a large number of small non-coding RNAs requires RNA polymerase II (Pol II) and the general transcription factors (GTFs) TFIIA, B, D, E, F and H that assemble into a large complex on the promoter DNA. This transcription preinitiation complex (PIC) is a key intermediate in Pol II transcription. *In-vitro* reconstitution studies of transcription initiation suggested a model in which PIC components assemble in a linear sequence (1,2). The first GTF that binds to the promoter is TFIID. TFIIA and TFIIB are then recruited followed by Pol II in association with TFIIF. Finally, TFIIE and TFIIH complete the formation of a PIC that is sufficient for basal *in-vitro* transcription but unable to drive activated transcription in response to specific activators. Important insights have been made on PIC architecture in yeast and human systems by biochemical and structural studies (3). A precise map of PIC locations across the yeast genome, including Pol II and GTFs, has been recently obtained, enabling the identification of TATA-like elements bound by TBP on TATA-less promoters and distinct PICs for divergent transcription (4,5).

Pol II transcriptional regulation requires additional multiprotein complexes, coactivators and corepressors, which modify the chromatin structure or directly contribute to PIC formation. Mediator of transcription regulation is one of these coregulators. While Mediator has been studied intensively, its complexity has precluded a detailed understanding of the molecular mechanisms of its action *in vivo*. Mediator is a huge complex (1.5 MDa) composed of 25–30 subunits depending on the organism that are organized into four structural modules: head, middle, tail and Cdk8 kinase modules. Recent electron microscopy studies redefined the modular organization of Mediator complex (6,7).

*To whom correspondence should be addressed. Tel: +33 1 69 08 54 13; Fax: +33 1 69 08 47 12; Email: julie.soutourina@cea.fr
Present addresses:
Sandra Wydau-Dematteis, EA 4065, CRP2, DHU Risks in pregnancy, Faculté de Pharmacie de Paris, Université Paris Descartes, Sorbonne Paris Cité, France.
Fanny Eyboulet, Institut de recherches cliniques de Montréal, 110 avenue des Pins Ouest, Montréal, Québec H2W 1R7, Canada.

Mediator subunits are engaged in numerous contacts within the complex (8–10). The large size, complexity and extreme flexibility have precluded the determination of a complete crystallographic structure of Mediator. Recently, structural data have been obtained for the yeast Mediator head module, the largest Mediator subcomplex characterized to date at high resolution (10,11).

Mediator transmits regulatory signals from specific transcription factors to the Pol II transcription machinery (12,13). This coregulator is generally required for Pol II transcription (14–18) and is present at most Pol II-transcribed gene promoters (19,20). Together with the GTFs, it promotes PIC formation and transcription initiation. Mediator also stimulates the phosphorylation of the Pol II carboxy-terminal domain (CTD) by TFIIH (21,22). Mediator cooperates with TFIID in yeast and human cells to stabilize the PIC (23–26). Previously, we have identified a direct contact between the Med11 Mediator head subunit and the Rad3 TFIIH subunit and showed that this contact is essential for the recruitment of the GTF to the PIC independently of Pol II (27). Recently, we showed that the Rpb3 Pol II subunit and the Med17 Mediator subunit are in direct contact to position Pol II on promoters and activate transcription, which strongly supports the notion that the Mediator–Pol II interaction is generally required for Pol II recruitment and transcription of class II genes in eukaryotes (28). Mediator was found to play an essential role in PIC assembly at the level of Pol II, TFIIH and TFIIE recruitment (27,28). Based on our results, we proposed a model of PIC assembly through multiple pathways (27).

Mediator is conserved in all eukaryotes (29) supporting a very ancient eukaryotic origin for this four-module complex. Given its central role in transcription regulation, it is not surprising that Mediator has been implicated in numerous developmental processes in animals, and mutations in Mediator subunits are involved in a number of pathologies (30,31). For example, a mutation in the Med23 subunit cosegregates with intellectual disability (32). In line with the fact that oncogenesis results from gene disregulation, Mediator has been found to be involved in several cancers (33–38).

Med17 is one of the ten essential yeast Mediator subunits. *MED17* was initially isolated as *SRB4*, one of the *SRB* genes whose mutations suppressed the growth phenotype of truncations of the Pol II Rpb1 CTD (39). The general requirement of Mediator for Pol II transcription has been shown using the *med17-138* mutant that generally affects Pol II transcription in a manner comparable with that of the *rpb1-1* Pol II mutant (14). This classical *med17* temperature-sensitive (ts) allele causes dissociation of the head module from the rest of Mediator leading to a loss of Mediator function at the restrictive temperature (40–42). The central role of the Med17 subunit in Mediator's function is also consistent with a central and extended positioning of this subunit within the Mediator head structural model (10). The importance of the Med17 subunit's role has been highlighted by the fact that a mutation in this subunit has been associated with infantile cerebral atrophy (43) and because of this subunit's involvement in cancer (37).

We aimed to enhance our understanding of the key mechanisms that allow Mediator to stimulate PIC formation *in vivo* at the genomic scale. We chose a strategy using temperature-sensitive mutants that allow the study of essential Mediator subunits providing specific changes in Mediator function without a complete loss or disassembly of Mediator. In this work, we have obtained a detailed genome-wide view of Mediator's role in PIC assembly *in vivo* by characterizing our large collection of conditional ts mutants in the Med17 Mediator head subunit. A mutant of yeast Med17 proposed to be equivalent to the human Med17-L371P responsible for infantile cerebral atrophy, which has a severe ts phenotype, was also included in our analysis. We show that *med17* mutations, which do not have a major effect on Mediator stability, differentially affect the genome-wide occupancy of PIC components. This work suggests that Mediator independently orchestrates multiple steps of the PIC assembly pathway.

MATERIALS AND METHODS

Strains and plasmids

All *S. cerevisiae* strains are described in Supplementary Table S1. All plasmids are listed in Supplementary Table S2. The oligonucleotides used in this study can be found in Supplementary Table S3.

ChIP and ChIP-seq

ChIP experiments were performed as described previously (44). Cell cultures (100 ml) were grown to exponential phase in YPD medium at 30°C, transferred for 45 minutes to a shaking incubator set at 37°C to allow gradual warming and cross-linked with 1% formaldehyde for 10 min. The 3HA-tagged proteins were immunoprecipitated with 12CA5 antibody and Pol II with 8WG16 anti-CTD antibody (Covance), bound to IgG magnetic beads (Dynabead). ChIP-seq experiments were performed as described previously (45). Chromatin preparation for ChIP-seq experiments was performed as described previously for conventional ChIP, except that an additional sonication step with Bioruptor (Diagenode, 6 cycles of 30s with medium intensity setting) was included to generate DNA fragments of ∼200 bp mean size. DNA sequencing of 40 nt-tags was performed on a Solexa genome analyzer GA-IIx or Hi-Seq using the procedures recommended by the manufacturer (Illumina). Input DNA and DNA from ChIP with an untagged strain were used as negative controls. Mediator ChIP-seq analysis was performed only for the Med15 subunit. Low ChIP signals were obtained for the Med8-HA subunit. High background levels in the ChIP-seq experiments for Med5-HA and Med6-HA subunits precluded accurate enrichment detection. It should be noted that Mediator enrichment levels in ChIP experiments are relatively low, depending on the Mediator subunit used, possibly due to the low efficiency of formaldehyde crosslinking and/or the dynamic association of Mediator to chromatin.

The ChIP-seq data have been deposited to the Array Express under accession numbers E-MTAB-2961 for the mutant strains and E-MTAB-1595 for the wild-type (WT) strain.

Coimmunoprecipitation experiments

Whole yeast extracts were prepared from 100 ml of cells grown to exponential phase in YPD medium at 30°C. When indicated, the cells were then transferred for 45 min to 37°C. Whole yeast extract preparation, immunoprecipitation (IP) in IP buffer (50 mM HEPES, pH 7.5, 100 mM NaCl, 20% glycerol, 1 mM dithiothreitol, 0.5 mM EDTA, 0.05% NP-40) supplemented with a protease inhibitor cocktail (Complete, Roche) and 1 mM PMSF and western blotting were performed as described previously (46). The 12CA5 anti-HA antibodies were used against HA-tagged proteins; rabbit polyclonal anti-Med14 and anti-Med17 antibodies were used against corresponding N-terminal peptides to detect Med14 and Med17 Mediator subunits, respectively.

Formaldehyde cross-linking experiments were performed as described previously (28). Briefly, cells were cross-linked with 1% formaldehyde for 10 min, as described for ChIP. Lysis was performed in 0.5 ml FA/SDS buffer in the presence of glass beads (0.75 ml, 425 to 600 μm) by vortexing for 45 min at 4°C. Crude extract preparation and IP were performed as described for conventional CoIP except that the immune complexes were washed as described for ChIP. A sonication step was added to recover chromatin-associated proteins. Denaturing conditions (8 M urea for 20 min at room temperature, cooled to 4°C and diluted with lysis buffer to a final urea concentration of 2 M) were used before IP to dissociate the subunits of Pol II and Mediator.

Mediator purification

Mediator purification was performed following a procedure adapted from Cai *et al.* (47) with some modifications. Med17 mutant and WT strains derived from CA001 protease-deficient background were grown at 30°C in 1 liter of 2×YPD medium overnight to late exponential phase. Cells were collected by centrifugation, washed twice in distillated water, resuspended in a buffer (1 ml/g of cells) containing 0.25 M Tris–HCl, pH7.6, 0.3 M ammonium sulfate, 2 mM EDTA, 30% glycerol, 5 mM 2-mercapthoethanol supplemented with 2× protease inhibitor cocktail (Complete, Roche) and frozen with liquid nitrogen. To prepare whole cell extract, cells were disrupted in an Eaton-Press. After thawing, the extract was clarified by ultracentrifugation (4°C, 1 h, 40 000g). The clear extract was submitted to a selective ammonium sulfate precipitation to isolate the 30–55% fraction. All buffers used for purification were supplemented with a protease inhibitor cocktail except for TEV digestion buffer. The precipitate was resuspended in IgG binding buffer (25 mM sodium phosphate buffer, pH7.5, 200 mM potassium acetate, 1 mM EDTA, 10% glycerol, 5 mM 2-mercapthoethanol) and incubated for 3 h with 100 μl of IgG-coated beads (GE Healthcare) in poly-prep columns (BioRad) at 4°C on a rotator. Beads were drained by gravity and washed with 10 ml of IgG wash buffer I (50 mM sodium phosphate buffer, pH 7.5, 500 mM ammonium sulfate, 1 mM EDTA, 10% glycerol, 5 mM 2-mercapthoethanol), followed by a wash with 10 ml of IgG wash buffer II (50 mM sodium phosphate buffer, pH 7.5, 100 mM ammonium sulfate, 1 mM EDTA, 10% glycerol, 5 mM 2-mercapthoethanol) and 10 ml of TEV digestion buffer (50 mM sodium phosphate buffer, pH 7.5, 100 mM potassium acetate, 1 mM EDTA, 10% glycerol, 5 mM 2-mercapthoethanol). Beads were incubated overnight with 20 U of TEV protease (Life Technologies) in 400 μl of TEV digestion buffer. The eluate was recovered, diluted 6-fold in Ni-NTA binding buffer (50 mM sodium phosphate buffer, pH 7.5, 0.01% NP-40, 10% glycerol, 500 mM potassium acetate, 10 mM imidazole) and incubated for 3 h on a rotator at 4°C with 100 μl of Ni-NTA sepharose beads (GE Healthcare) on poly-prep columns. Beads were drained by gravity and washed with 10 ml of Ni-NTA wash buffer (50 mM sodium phosphate buffer, pH 7.5, 0.01% NP-40, 10% glycerol, 500 mM potassium acetate, 40 mM imidazole). The Mediator complex was eluted with 200 μl of Ni-NTA elution buffer (50 mM sodium phosphate buffer, pH 7.5, 0.01% NP-40, 10% glycerol, 500 mM potassium acetate, 200 mM imidazole), and flash-frozen after addition of 10% glycerol to a final glycerol concentration of 20%.

The presence of selected Mediator subunits (Med8-HA, Med14, Med17 and Med21) was verified by western blotting with anti-HA antibody (12CA5), polyclonal rabbit anti-Med14, anti-Med17 or anti-Med21 antibodies. Purified Mediator complex was then analyzed using a mass-spectrometry approach.

Mass spectrometry analysis

To analyze Mediator integrity in *med17* mutants, Mediator was immunoprecipitated from crude extracts of Med5-HA tagged strains as described for CoIP experiments, except that protein G magnetic beads were used instead of IgG magnetic beads (Dynabead) and the elution was performed for 20 min at 65°C instead of 2 min at 85°C. The *MED17* strain carrying the non-tagged Mediator subunit was used as a negative control. Proteins from each eluate were separated by SDS-PAGE to fractionate the protein samples into three fractions and exclude the regions corresponding to heavy and light IgG chains. The gels were stained with Coomassie Blue and each fraction was cut into bands of ∼2 mm and subjected to in-gel trypsin digestion with the Progest robot (Genomic Solutions, Chelmsford, MA) using standard conditions including reduction and alkylation. To analyse the purified Mediator complex, a short migration in NuPage 4–12% gel (Life Technologies) was performed before mass spectrometry analysis. After overnight tryptic digestion, peptides were extracted with 60% acetonitrile and 0.1% (v/v) formic acid. Tryptic peptides extracted from different bands of three gel regions were pooled, vacuum dried and resuspended in 0.1% (v/v) formic acid prior to nanoLC–MS/MS mass spectrometry analyses. The same cutting pattern of the SDS-PAGE lane was performed for each eluate.

The nanoLC–MS/MS analyses were performed with the Triple-TOF 4600 mass spectrometer (AB Sciex, Framingham, MA, USA) coupled to the nanoRSLC ultra performance liquid chromatography (UPLC) system (Thermo Scientific) equipped with a trap column (Acclaim PepMap100C18, 75 μm i.d. × 2 cm, 3 μm) and an analytical column (Acclaim PepMapRSLCC18, 75 μm i.d. × 15 cm, 2 μm, 100 Å). Peptide separation was performed with a 5–35% solvent B gradient for 40 min. Solvent A was 0.1% formic acid in water, and solvent B was 0.1%

formic acid in 100% acetonitrile. The nanoLC–MS/MS experiments were conducted using the data-dependent acquisition method by selecting the 20 most intense precursors for CID fragmentation with Q1 quadrupole set at low resolution for better sensitivity. Raw data were processed using MS Data Converter software (AB Sciex) for generating .mgf data files and protein identification was performed using the MASCOT search engine (Matrix science, London, UK) against the Swissprot database (release 2014_08) with carbamidomethylation of cysteines and oxidation of methionines set as fixed and variable modifications, respectively. Peptide and fragment tolerance were respectively set at 20 ppm and 0.05 Da. Results were analyzed using Scaffold 3.6.5 software (Proteome Software). Only proteins with at least two unique peptides and a 95% probability for both peptide and protein identifications were considered.

Quantitative real-time PCR (qRT-PCR) analysis

RNA was extracted with hot acidic phenol following a protocol derived from Schmitt *et al.* (48). Reverse transcription of 0.5 μg RNA samples was performed using an iScript cDNA synthesis kit (BIO-RAD) with a mixture of oligo(dT) and random hexamers for priming. qRT-PCR results were normalized using *25S* rRNA, *18S* rRNA and *SCR1* Pol III-synthesized RNA as internal controls. Values represent the average of three independent experiments, and error bars indicate standard deviations.

Data analysis

ChIP-seq data were analyzed as described previously (45). The sequences were aligned on the *S. cerevisiae* genome (UCSC version sacCer3) using Bowtie version 0.12.7 (49). Only uniquely mapped tags were used and a maximum of two mismatches was allowed. Conversions to different file formats were performed using Samtools version 0.1.16. To avoid possible sequencing artifacts, reads with the best-quality scores were conserved for each position. The number of mappable tags for each ChIP-seq experiment is indicated in Supplementary Table S4.

To calculate ChIP-seq density, reads were extended to an assumed fragment length of 150–180 nt, and a count of reads was determined per 1-bp bin using Bedtools version 2.15.0. ChIP-seq density profiles were displayed using the Integrated Genome Browser (IGB) yeast genome browser. Input DNA and DNA from ChIP with an untagged strain were used as negative controls. The ChIP sample from the untagged strain generally shows very low tag density on the genome, except for some regions representing <1% of the genome that displays an apparent enrichment. It should be noted that the majority of these regions were located inside the highly transcribed class II genes. To correct for this non-random background distribution, we subtracted the normalized signal of the untagged strain sample from the ChIP samples for each protein. The ChIP signals of the untagged strain have different impacts on the ChIP signals for different proteins. For this reason, the subtraction step was preceded by a normalization of the ChIP signal of an untagged strain compared with the corresponding ChIP sample based on the qPCR analyses of nontranscribed control regions. The normalization values for untagged strain sample before subtraction are indicated in Supplementary Table S5.

The significantly enriched regions were identified using peak calling MACS2 software version 2.0.10.20120703 (50). To avoid possible sequencing artifacts, reads beyond five repetitions at the same position of the genome were removed. A minimum false discovery rate (*q*-value) cutoff peak detection of 0.01 was used for Med15 and 0.05 for Pol II, Rad3, Kin28 and TBP. This step was followed using the PeakSplitter step of PeakAnalyzer software for the subdivision of ChIP-seq regions into discrete peaks (51). The significantly enriched regions were also identified in the control ChIP sample with an untagged strain using Bayespeak version 1.10.0 (52) with a threshold of 0.9. Around 200 peaks were identified by this method in the control sample and they were used to correct peakcalling data from Med15, Rad3, Kin28 and TBP ChIP-seq.

GTFs, Mediator and Pol II significantly enriched peaks were annotated relative to the intergenic region or the ORF in which they were detected using BedTools version 2.15.0. The nomenclature used for the intergenic regions was as follows: tandem regions were named relative to the downstream-located gene, divergent and convergent regions were named relative to the two genes surrounding the region.

To compare read counts in WT and *med17* mutant ChIP-seq data, a count of reads was determined on promoter regions of Pol II-transcribed genes for Rad3, Kin28, TBP and Med15, and on Pol II-transcribed gene ORFs for Pol II, using Bedtools. For ChIPseq data analysis, promoter regions were defined as corresponding intergenic regions on the yeast genome. For this step, all mapped reads were conserved to allow quantitative comparison between the different samples. Read numbers were normalized relative to qPCR data on a set of selected regions (Supplementary Table S6) using the ratio between WT and mutant strains. The ratio of ChIP-qPCR values (V) between WT and mutant strains was calculated for each selected region ($R_{\mathrm{qPCR}} = V_{\mathrm{qPCRmut}}/V_{\mathrm{qPCRwt}}$). In parallel, the ratio of ChIP-seq reads (N) between WT and mutant strains was determined for the same region ($R_{\mathrm{seq}} = N_{\mathrm{seqmut}}/N_{\mathrm{seqwt}}$). The normalization coefficient between ChIP-qPCR and read ratios was then calculated for each region ($Q = R_{\mathrm{qPCR}}/R_{\mathrm{seq}}$). The median of normalization coefficients between ChIP-qPCR and read ratios was used for ChIPseq data normalization (Supplementary Table S7).

RESULTS

Collection of conditional *med17* Mediator mutants

Previously, to investigate the *in-vivo* role of Med17 in Pol II recruitment, we selected a large collection of conditional *med17* mutants (28). The *med17* mutants with different thermosensitive phenotypes, from slow growth to lethal at non-permissive temperature (37°C), were generated by random mutagenesis (Supplementary Figure S1, Table S8). A number of multiple mutations were separated to obtain 5 additional point mutants by site-directed mutagenesis. An L371P mutation in the Med17 subunit has been

associated with infantile cerebral atrophy (43). A corresponding M504P mutation in the homologous *S. cerevisiae* Med17 (Supplementary Figure S2A) localized within one of the conserved domain based on multiple sequence alignments and secondary structure features (29) inactivated the protein at 37°C. To study the molecular consequences of this *med17* mutation, a *med17-504* yeast strain carrying a *med17-M504P* mutation was constructed and the growth phenotype of this mutant was investigated. Figure 1A shows that *med17-504* leads to a slow growth phenotype at 30°C and a strong thermosensitive phenotype at 37°C. In total, a collection of 30 conditional mutants in the Med17 subunit was obtained. The integrity of the main Mediator modules in all *med17* mutants has been verified by CoIP experiments (Supplementary Table S9). We decided to use this collection of Med17 Mediator mutants to investigate the *in-vivo* action of Mediator in general, and of the Med17 subunit in particular in PIC formation.

Effects of *med17* mutations on Mediator stability, interaction with Pol II and mRNA level

Four mutants were selected for further study based on their growth phenotypes (normal or slightly slower growth at 30°C combined with pronounced ts phenotype at 37°C), Mediator integrity and low mutation number: *med17-98 (L86Q, E186G, E448Q), med17-444 (Q444P), med17-504 (M504P)* and *med17-670 (V670E)* (Figure 1A). These four *med17* mutants all have mutations localized within or near the conserved domains of this subunit defined by a primary sequence comparison and predicted secondary structure (Supplementary Figure S2B) (29). The mutated amino acid residues of *med17* mutants were mapped on a partial structural model of the Mediator head module if the corresponding residues were present on the model (10) (Supplementary Figure S2C) and were found to often be located close to the module surface.

Since Mediator mutations can lead to dissociation of Mediator modules and a loss of Mediator function, the effect of *med17* mutations on the integrity of the main Mediator modules was first verified by CoIP experiments (Supplementary Figure S3A and Table S9). The HA-tagged Med5 Mediator subunit was immunoprecipitated with an anti-HA antibody. The coimmunoprecipitated Med17 Mediator head subunit and Med14 Mediator subunit bridging tail and middle modules were detected by western blotting with antibodies produced in house. Mediator head, middle and tail modules coimmunoprecipitated with the Med5 tail module subunit in all four mutants without any significant difference compared to the WT strain. We also performed CoIP experiments with whole yeast extracts prepared from cells grown to exponential phase in YPD medium at 30°C and then transferred for 45 min to 37°C (Supplementary Figure S3A). Similar to cells grown at 30°C, no significant differences were observed in *med17* mutants compared to the WT strain.

To investigate Mediator integrity in the selected *med17* mutants in more detail, Mediator was immunoprecipitated from crude extracts of Med5-HA tagged strains and immunoprecipitated proteins were analyzed using a mass spectrometry approach (Figure 1B, immunoprecipitation). To improve Mediator subunit identification using mass spectrometry, the immunoprecipitated proteins were separated on gel and the bands corresponding to IgG heavy and light chains were cut out. This procedure excluded some Mediator subunits with molecular weights close to those of the IgG chains. A strain carrying an untagged Med5 subunit was used as a negative IP control. Up to 19 Mediator subunits were identified belonging to all four Mediator modules. Thirteen Mediator subunits of head, middle, tail and Cdk8 modules (Med12, 13, 17, 6, 20, 1, 4, 7, 5, 14, 15, 16, 3) were present for all *med17* mutants and the WT strain. Mediator subunits with low molecular weight (Med9, 10, 11, 21, 22) were not detected in some samples. Mass spectrometry analysis thus showed the presence of Mediator head, middle, tail and Cdk8 modules for all *med17* mutants, indicating that mutations did not have a major effect on Mediator stability.

To improve our analysis of Mediator integrity in *med17* mutants, we purified Mediator complex by a two-step affinity purification method that allows to prepare core Mediator containing head, middle and tail modules but lacking Cdk8 module (47). Purified Mediator complex from the four *med17* mutants and a WT strain was assayed by SDS-PAGE (Figure 1C) and analyzed using a mass spectrometry approach. Yeast core Mediator is composed of 21 subunits since it lacks the 4 Cdk8 module subunits. The Med31 Mediator subunit escaped mass spectrometric identification (8), leading to 20 core Mediator subunits that could be detected by this approach. Our mass spectrometry analysis showed that all 20 Mediator subunits were present in Mediator complex purified from *med17* mutants and a WT strain (Figure 1B, Mediator purification). Even though no peptides were initially detected for Med21 subunit (a small Mediator subunit of 16 kDa) in *med17-98* mutant, the presence of this subunit in *med17-98* Mediator complex was confirmed by a second data acquisition identifying 2 unique peptides and our western blotting analysis with anti-Med21 antibody (Supplementary Figure S3B). Taken together, our data strongly suggest that *med17-98, 444, 504 and 670* mutations did not compromise Mediator integrity.

The Med17 Mediator subunit directly interacts *in vivo* with the Rpb3 Pol II subunit (28). As described previously (28), CoIP experiments for Mediator–Pol II interaction are not appropriate to investigate the effect of mutations since their effects depend on the buffer conditions. Hence the need to determine how Mediator Med17 mutations affect the specific Med17–Rpb3 contact using a formaldehyde-crosslinking approach with IP under denaturing conditions. This method was used in our previous work to show an impaired Med17–Rpb3 contact in an *rpb3-2* mutant (28). We examined whether this contact was modified in *med17* mutants. For these experiments, yeast strains were constructed carrying an EGFP-tagged Med17 subunit and an Myc-tagged Rpb3 subunit in WT and *med17* mutant contexts. Proteins were cross-linked with formaldehyde, the Med17-EGFP-tagged subunit was immunoprecipitated under denaturing conditions and the cross-linked Rpb3-Med17 band was detected with an anti-Myc antibody (Figure 1D, red arrow). The results demonstrated that Rpb3–Med17 contact was strongly reduced in the *med17-504* mutant (Figure 1D), but remained largely unchanged

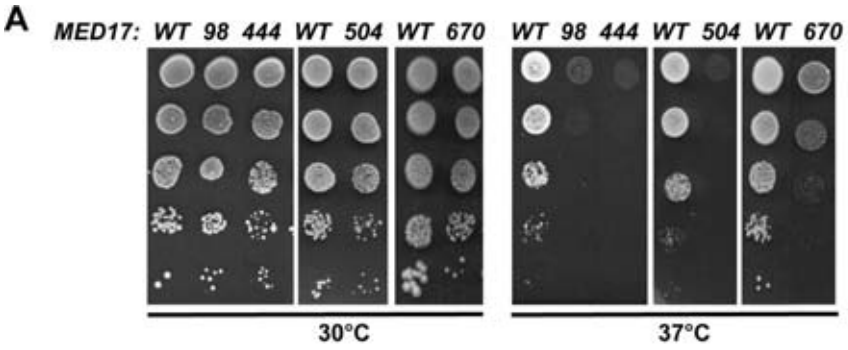

B

			Number of unique peptides										
			Immunoprecipitation						Mediator purification				
Yeast protein	Module	Molecular Weight	Med17 -WT	Med17 -98	Med17 -444	Med17 -504	Med17 -670	C	Med17 -WT	Med17 -98	Med17 -444	Med17 -504	Med17 -670
Med12	Cdk8	167kDa	5	4	2	5	13	0	0	0	0	0	0
Med13	Cdk8	160 kDa	3	6	5	3	10	0	0	0	0	0	0
Med17	Head	78 kDa	10	12	11	13	13	0	24	14	16	12	46
Med18	Head	34 kDa	5	1	0	1	4	0	5	7	5	3	15
Med6	Head	33 kDa	5	1	1	1	3	0	4	5	1	3	11
Med8	Head	25 kDa	0	0	0	0	0	0	3	2	1	1	9
Med19	Head	25 kDa	0	0	0	0	0	0	2	1	1	2	4
Med20	Head	23 kDa	6	5	3	6	5	0	6	9	8	3	12
Med22	Head	14 kDa	2	1	0	1	2	0	2	4	2	1	5
Med11	Head	13 kDa	1	1	0	1	2	0	4	6	3	2	9
Med1	Middle	64 kDa	12	11	7	9	14	0	9	11	10	4	26
Med4	Middle	32 kDa	8	6	7	4	9	0	7	11	8	7	18
Med7	Middle	26 kDa	3	4	1	3	4	0	4	5	5	2	9
Med10	Middle	18 kDa	2	0	1	4	1	0	5	4	2	4	7
Med9	Middle	17 kDa	0	0	0	0	2	0	5	2	3	4	7
Med21	Middle	16 kDa	3	0	0	0	2	0	2	*	1	2	5
Med5	Tail	129 kDa	35	34	30	36	38	3	17	29	18	12	52
Med14	Tail	123 kDa	22	17	17	22	25	0	30	27	24	23	53
Med15	Tail	120 kDa	10	9	11	12	16	0	9	12	13	9	32
Med16	Tail	111 kDa	37	39	32	40	44	0	12	27	17	10	56
Med2	Tail	48 kDa	0	0	0	0	0	0	2	1	1	2	8
Med3	Tail	43 kDa	3	2	2	2	5	0	4	3	2	1	5

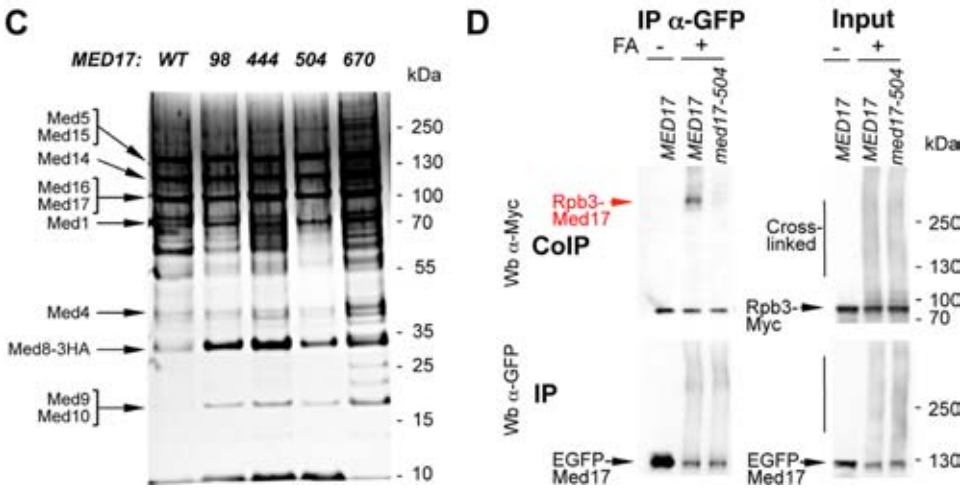

Figure 1. *med17* thermosensitive mutants. (**A**) Med17 mutant phenotypes. Cultures of WT and mutant *med17* yeast strains were serially diluted, spotted on YPD agar plates and incubated for 3 days at permissive (30°C) or non-permissive (37°C) temperatures. (**B**) Mass spectrometry analysis of Mediator integrity in *med17* mutants. Mediator subunits identified by mass spectrometry analysis in WT and *med17* mutants are indicated. (Immunoprecipitation) Mediator was immunoprecipitated through Med5-HA from crude extracts using magnetic protein G beads coupled to anti-HA antibodies. The *MED17* strain carrying a non-tagged Mediator subunit was used as a negative control (C for Control IP). (Mediator purification) Core Mediator complex containing head, middle and tail modules was purified from *med17* mutants and a wild-type strain. An asterisk marks Med21 subunit in *med17-98* mutant that was detected in a second data acquisition identifying two unique peptides and also by western blotting with anti-Med21 antibody (Supplementary Figure S3B). (**C**) Silver-stain SDS-PAGE analysis of purified Mediator complex from the WT strain and *med17* mutants. (**D**) Interaction between Pol II and Mediator in *med17-504* mutant. Rpb3-Myc Med17-EGFP strains with WT *MED17* or a *med17* mutation were grown at 30°C in YPD medium and cross-linked or not with formaldehyde (FA), as indicated. Med17-EGFP was immunoprecipitated (IP) with anti-EGFP antibody from crude extracts (Input) and analyzed by western blotting with anti-Myc antibody (CoIP) against Rpb3. The cross-linked Rpb3-Med17 band is indicated in red. The position of unidentified cross-linked proteins with the tagged Med17 or Rpb3 subunits is indicated by a vertical bar.

in *med17-98*, *444* and *670* compared to the wild type (Supplementary Figure S4).

The effect of *med17* mutations after a transfer to 37°C on mRNA abundance of *ADH1*, *PYK1* and *PMA1* genes was investigated (Supplementary Figure S5). The *med17-98, 444 and 670* mutants were found to affect the level of these mRNAs. The effect of *med17-98* was accentuated at 37°C and that of other mutations was essentially similar at 30°C and 37°C. It should be noted that *med17-504* shows little, if any, effect on the steady-state levels of the three mRNAs. As the measurement of mRNA levels is a cumulative result of RNA synthesis and RNA turnover, mRNA levels do not fully reflect the effects of *med17* mutations on transcription. Moreover, it has been shown recently that cells can compensate for global transcription changes by RNA degradation changes to buffer cellular mRNA levels (53,54). We measured Pol II occupancy on transcribed regions by ChIP since it indicates transcriptional activity in yeast (55,56).

Mutations in Med17 differentially affect chromatin association of PIC components on selected constitutively expressed genes

To analyse the molecular effect of *med17* mutations on PIC formation, occupancy of Pol II, GTFs and Mediator was determined by ChIP on selected constitutively expressed genes. Yeast strains grown in YPD-rich medium and transferred to a non-permissive temperature (37°C) for 45 min were used for chromatin preparation. The association of Mediator was measured by ChIP experiments with three different Mediator subunits: Med6-HA (head), Med15-HA (tail) and Med5-HA (tail) (Figure 2A–C). The Mediator occupancy of the *ADH1*, *PYK1* and *PMA1* promoter regions remained largely unchanged except for Med15 Mediator occupancy that was reduced in the *med17-444* mutant and to some extent for other mutants on the *PMA1* promoter region. In contrast, all examined mutations led to a decrease in Pol II association with the promoter and transcribed regions of class II genes compared to the WT (Figure 2D), with *med17-444* and *med17-504* showing the most pronounced effect, reflecting the effects on Pol II transcription.

With the Mediator head module directly interacting with TFIIH and TBP, the ability of *med17* mutations to influence the occupancy of these GTFs was assessed *in vivo*. Two TFIIH modules, TFIIH core (Rad3-HA subunit) and TFIIK kinase module (Kin28-HA) were ChIPed (Figure 2E and F). Interestingly, mutations in the Med17 Mediator subunit were found to differentially affect the presence of the two TFIIH modules on the *ADH1*, *PYK1* and *PMA1* promoters. In the *med17-98* and *med17-504* mutants, Med17 mutations led to a decrease in the occupancy of both TFIIH modules. The *med17-444* mutation specifically affected Kin28 occupancy. More unexpectedly, a decrease in Rad3 occupancy without any effect on Kin28 occupancy was observed in *med17-670,* suggesting that TFIIH modules can behave independently *in vivo*.

TBP occupancy in *med17* mutants was also analyzed (Figure 2G). As previously observed for *med11* Mediator mutants, TBP occupancy was similar to that of the WT strain in *med17-98* and *670* mutants. In contrast, TBP association to the *ADH1, PYK1* and *PMA1* gene promoters was reduced in *med17-444* and *med17-504* indicating that Mediator could affect the recruitment and/or stability of this GTF *in vivo*.

Effects of *med17* mutations on chromatin occupancy of PIC components on the inducible *GAL1* gene

To address the recruitment of PIC components to an inducible yeast gene, ChIP experiments were performed with Mediator, Pol II and GTFs in *med17* mutants on the *GAL1* gene. The association of Mediator (Med5 subunit), Pol II, TFIIH core (Rad3 subunit), TFIIH kinase module (Kin28 subunit) and TBP were analyzed by ChIP at 45 min of galactose induction (data not shown). The association of PIC components was generally affected in the same manner as for the three constitutively expressed genes, with *med17-504* being an exception with reduced Mediator recruitment and unmodified Rad3 and TBP recruitment to the *GAL1* promoter region at 45 min of galactose induction.

Two *med17* mutants were chosen for further experiments to address the kinetics of the *GAL1* gene induction: *med17-444*, since it is the only mutant that affected TBP recruitment to the *GAL1* promoter and *med17-504*, since its effects on the *GAL1* gene differ from those on the *ADH1*, *PYK1* and *PMA1* genes for several PIC components. Yeast cells were grown in YP raffinose medium at 30°C, then galactose was added at the 0 time point and cultures were transferred to 37°C. Samples were collected at 0, 20, 40 and 60 min of galactose induction and transfer to 37°C. The kinetics of Mediator, Pol II and TBP recruitment upon galactose induction were analyzed in *med17-444* and *-504* mutants compared to the wild type (Figure 3). Mediator recruitment was decreased in *med17-504* for all kinetics points, showing a particular Mediator behavior on the *GAL1* gene in this mutant (Figure 3A). In the *med17-444* mutant, Mediator occupancy of the *GAL1* gene promoter reached a level similar to that in the wild type, even though the kinetics of Mediator recruitment were slower (20-min point). Pol II occupancy generally followed that of Mediator (Figure 3B). The *med17-444* mutation was found to slow TBP recruitment during galactose induction and *med17-504* showed TBP recruitment kinetics similar to that of the WT strain (Figure 3C).

Taken together, the ChIP results demonstrate that mutations in the Med17 Mediator subunit could differentially affect the recruitment of PIC components and also highlight some gene-specific effects suggesting that regulatory mechanisms might differ depending on particular Pol II-transcribed genes.

Genome-wide location analysis of Mediator, Pol II, TBP and TFIIH modules

To extend the ChIP analysis of PIC assembly to the whole yeast genome, ChIP-seq experiments were performed for Mediator (Med15 subunit), Pol II and GTFs (TBP and two TFIIH subunits: Kin28 and Rad3). Input DNA and DNA from ChIP with an untagged strain were used as negative controls. Figure 4A shows examples of ChIP-seq density distributions using the IGB for all proteins on selected

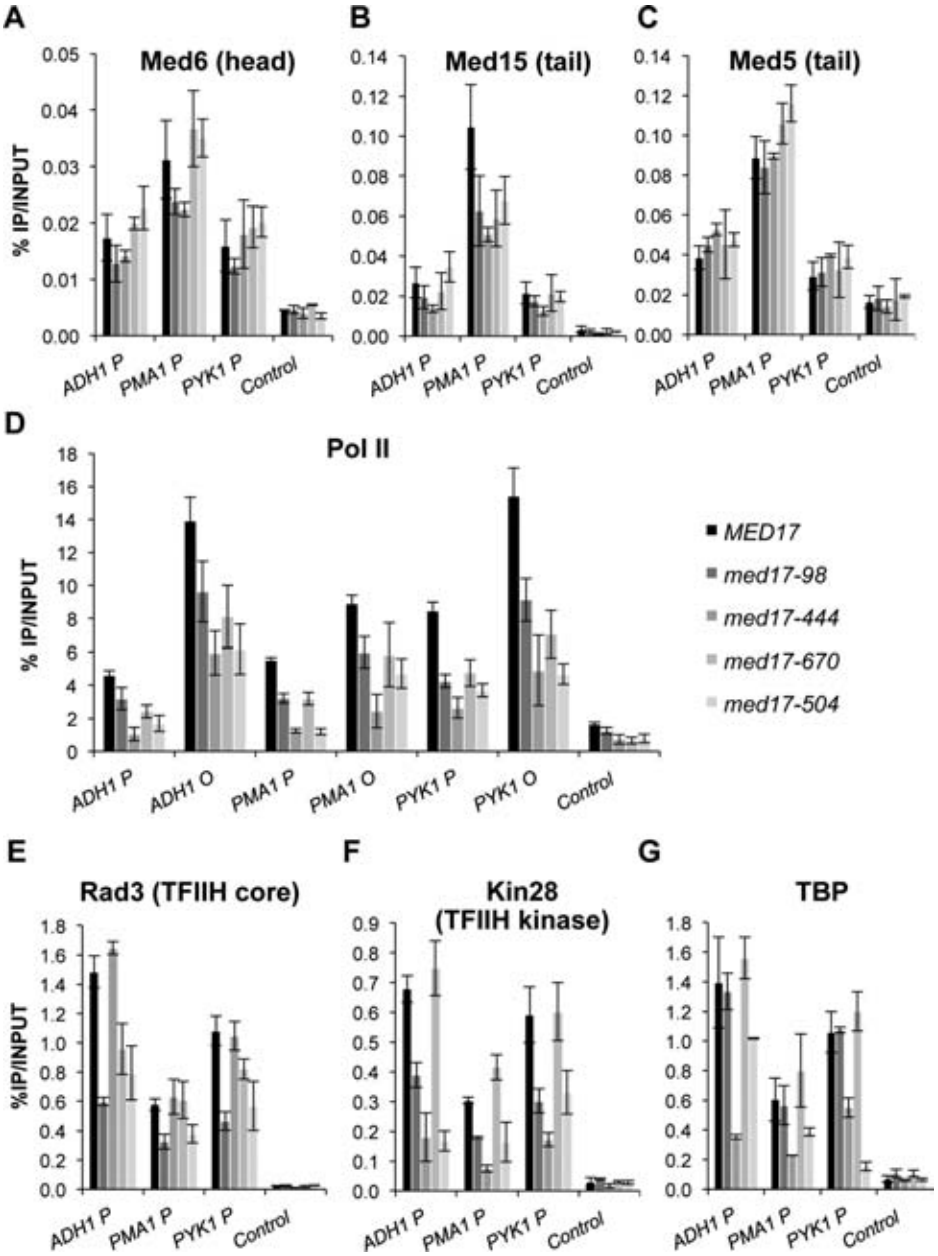

Figure 2. Effect of *med17* mutations on Mediator, Pol II, TFIIH and TBP occupancy. Cells were grown to exponential phase at 30°C on YPD medium and then transferred for 45 min to 37°C. Quantitative ChIP experiments were performed using anti-HA antibody (12CA5) against Mediator subunits Med6-HA (**A**), Med15-HA (**B**) or Med5-HA (**C**), Rad3-HA (**E**), Kin28-HA (**F**), TBP-HA (**G**) or anti-Rpb1 Pol II antibody (8WG16) (**D**). Immunoprecipitated DNA was amplified with primers corresponding to *ADH1, PMA1* and *PYK1* ORF (O) or promoters (P). P1 primers listed in Supplementary Table S3 located close to upstream regulatory regions were used for Mediator ChIP experiments and P2 primers located close to core promoters were used for Pol II, Rad3, Kin28 and TBP ChIP experiments. *GAL1* ORF was used as a negative control. The mean values and standard deviation (indicated by error bars) of three independent experiments are shown.

class II genes in WT strains. To correct for chromatin-state bias corresponding to the highly expressed genomic loci observed for control samples (15,45,57–59), the normalized signals of an untagged strain sample were subtracted from the ChIP samples for each protein as described previously (45) and in the 'Materials and Methods' section. The ChIP signals of Mediator inside ORFs most likely resulted from chromatin-state bias and are mostly corrected by untagged strain signal subtraction.

The location of Mediator, Pol II and GTF peaks were compared around transcription start sites (TSS) in WT strains in a metagene analysis (Figure 4B). To consider only Pol II transcribed gene promoters, intergenic regions encompassing Pol III-transcribed genes were excluded. Divergent genes with double peaks for GTFs were also excluded from the analysis. Mean tag density (1 bp bin) was determined for each protein in a 1600-bp window centred on the TSS. These analyses show that the ChIP-seq distributions of

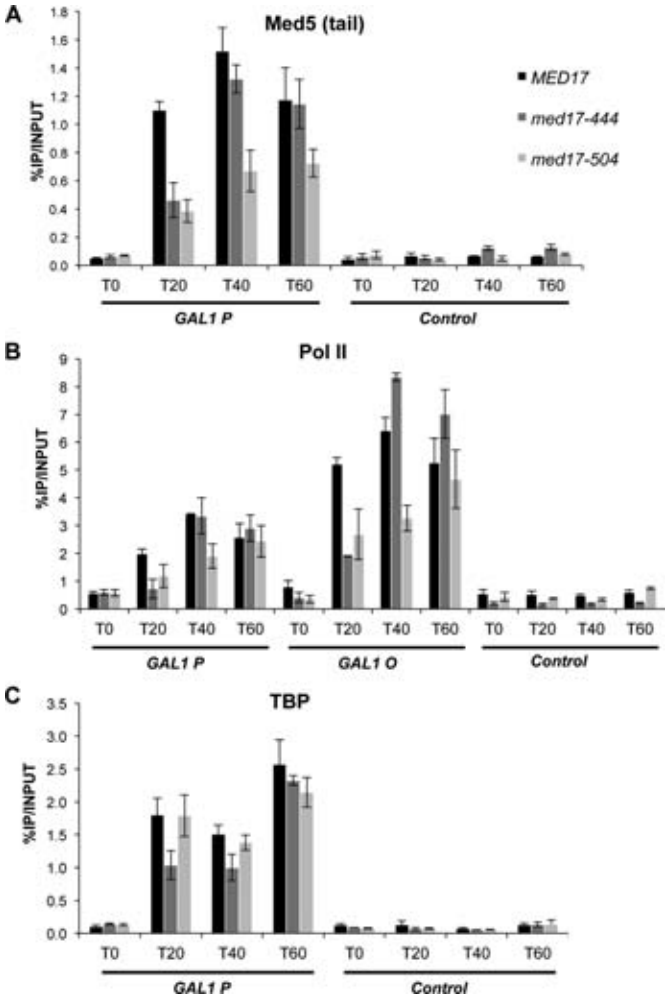

Figure 3. Kinetics of galactose induction in *med17-444, -504* and WT strains. Yeast strains were grown in raffinose-supplemented medium at 30°C, then galactose was added, cultures were transferred at the same time to 37°C and samples were collected for ChIP experiments at indicated time points upon galactose induction (T0, T20, T40 and T60 min). Quantitative ChIP experiments were performed using anti-HA antibody (12CA5) against Mediator subunit Med5-HA (**A**), TBP-HA (**C**) or anti-Rpb1 Pol II antibody (8WG16) (**B**). The mean values and standard deviation (indicated by error bars) of three independent experiments are shown. Immunoprecipitated fragments from ChIP experiments were amplified with primers corresponding to the *GAL1* gene promoter (*GAL1 P*) or ORF (*GAL1 O*). A nontranscribed region on chromosome V was used as a negative control.

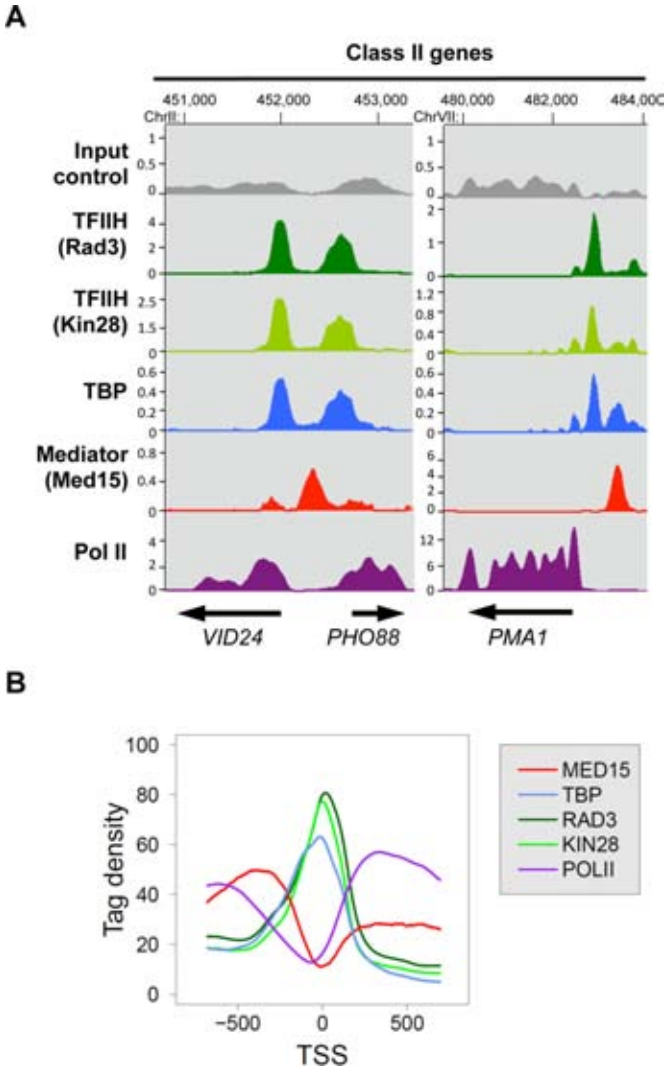

Figure 4. Enrichment profiles of Mediator, Pol II, TFIIH and TBP on yeast genome. Cells were grown at 30°C in YPD medium and then transferred for 45 minutes to 37°C. (**A**) Examples of Mediator, Pol II, TBP, and TFIIH ChIP-seq enrichment profiles on selected class II genes. Densities of sequence tags were assessed from ChIP-seq experiments performed with Med15-HA (Mediator), TBP-HA, Rad3-HA (TFIIH core), and Kin28-HA (TFIIK) strains using anti-HA antibody. Pol II was immunoprecipitated using anti-Rpb1 antibody. ChIP-seq density profiles are displayed using the IGB yeast genome browser. Input DNA and DNA from ChIP with an untagged strain were used as negative controls. Densities of sequence tags were displayed after subtraction of the normalized control of an untagged strain. The scales in kiloreads are indicated for each profile. (**B**) Distribution of Mediator, TBP, TFIIH and Pol II ChIP-seq densities around TSS. Intergenic regions encompassing Pol III-transcribed genes and divergent genes were excluded. The tag density was determined for each protein in a 1600-bp window centred on the TSS. The TSS positions were provided from previous studies (4,5). Mean tag density for each nucleotide position was then calculated and plotted over the window.

TFIIH subunits and TBP superposed with each other close to TSS. As expected, Pol II is distributed inside transcribed regions. Mediator distribution was located upstream of TSS on regulatory regions.

med17 mutations can globally destabilize the PIC *in vivo*

To investigate whether PIC assembly is generally affected in *med17* mutants or in a gene-specific manner, the genome-wide occupancy of Mediator, Pol II and GTFs were analyzed using ChIP-seq experiments in mutants to compare them with the WT strains. Cells were grown at 30°C in YPD medium and then transferred for 45 min to 37°C. The normalization step is essential for ChIP-seq comparative analysis, but widely used normalization methods like a quantile normalization step cannot be applied in situations where occupancy increases or decreases genome-wide. To detect the potential global effects of Mediator mutations on PIC component occupancy, we performed the following normalization step. A count of reads was determined on the promoter regions of Pol II-transcribed genes for Med15, Rad3, Kin28 and TBP, and on Pol II-transcribed gene ORFs for

Pol II and then normalized relative to qPCR data on a set of selected regions, as described in the 'Materials and Methods' section. Regression analysis of PIC component binding in each *med17* mutant versus WT was systematically performed.

Genome-wide Mediator occupancy was analyzed for the Med15 Mediator subunit. It was not possible to obtain good quality ChIP-seq results for the Med5 Mediator tail module subunit or the Med6 and Med8 Mediator head module subunits (see 'Materials and Methods' section). Chromatin associated with the Med17 Mediator head subunit can be ChIPed efficiently. However, the addition of tags to mutant subunits has been observed to potentially lead to an aggravation of growth phenotypes. For this reason, Med17 occupancy was not investigated in mutant strains.

The ChIP results on the selected class II genes showed the most pronounced effects on Pol II, TBP and Kin28 occupancy for the *med17-444* mutant whereas Rad3 occupancy remained unaffected in this mutant (Figures 2 and 3). Genome-wide analysis of the *med17-444* mutant revealed a global 1.8-fold decrease (the slope of regression line, shown in red, is equal to 0.55) in Med15 Mediator occupancy with a high correlation coefficient (R^2 equal to 0.93) (Figure 5A). As a consequence, the presence of other PIC components like Pol II, TFIIH and TBP was also globally reduced to a different extent. A global decrease in genome-wide occupancy for Pol II and the Kin28 TFIIK subunit (2.6- and 2.7-fold, respectively) was observed. The TBP association to chromatin was also globally affected with a 1.6-fold decrease. The Rad3 TFIIH core subunit binding was slightly affected (1.2-fold decrease), consistent with the ChIP results on the *ADH1, PYK1* and *PMA1* gene promoters. Taken together, the genome-wide results on the *med17-444* mutant confirmed a central role for the Med17 Mediator subunit in PIC formation and suggested that the Mediator tail module destabilization on the chromatin could lead to a global change in the *in-vivo* binding of several PIC components but only marginally affected Rad3 occupancy.

The *med17-504* mutation was found to impair Pol II-Mediator interaction (Figure 1D) and led to reduced binding of Pol II and GTFs to the *ADH1, PYK1* and *PMA1* genes (Figure 2) and Mediator, Pol II and some GTFs on the *GAL1* gene (Figure 3 for Mediator, Pol II and TBP, and data not shown for TFIIH). To determine how general the effects of *med17-504* were, the genome-wide Mediator, Pol II, Rad3, Kin28 and TBP occupancy were compared in this mutant and the WT (Figure 5B). The genome–wide binding of the Mediator Med15 subunit in *med17-504* was similar to that of the WT strain (the slope equal to 0.93 and R^2 equal to 0.98). In contrast, the association of Pol II and the GTFs was globally diminished in this mutant compared to the WT, suggesting that the impaired Pol II–Mediator interaction leads to a general PIC assembly defect. The genome-wide analysis of *med17-444* and *-504* mutants demonstrated that a destabilization of Mediator binding to chromatin or an impaired interaction between Mediator and Pol II globally destabilize the PIC assembly *in vivo*.

Mutations in the Med17 Mediator subunit specifically affect the genome-wide association of the TFIIH core subcomplex

Previously, we have shown that mutations in the Med11 Mediator subunit affecting its interaction with the Rad3 TFIIH core subunit can selectively impair the binding of the TFIIH kinase module (27). Unexpectedly, the ChIP experiments suggested that some *med17* mutations like *med17-670* could lead to a selective dissociation of the Rad3 TFIIH core subunit. TFIIH core genome-wide binding in *med17* mutants was therefore investigated. The ChIP-seq results revealed that the genome-wide association of this TFIIH subcomplex was affected independently of the TFIIK subcomplex in *med17-670* (Figure 6A) and *-98* mutants (Figure 6B). A global 2-fold decrease of the Rad3 TFIIH core subunit binding was observed in these mutants with the slope of regression line equal to 0.55 and 0.51 for *med17-670* and *-98*, respectively, with high correlation coefficients. In contrast, the association of the Kin28 TFIIK subunit was similar to the WT level (the slope equal to 1.01 and 0.94, R^2 equal to 0.98 and 0.90 for *med17-670* and *-98*, respectively). The presence of the Med15 Mediator subunit was mostly unchanged or only slightly decreased (the slope equal to 0.87 and 0.80, R^2 equal to 0.93 and 0.94 for *med17-670* and *-98*, respectively). The genome-wide binding of TBP was not reduced and even showed a slight increase (the slope equal to 1.25 and 1.14, R^2 equal to 0.92 and 0.96 for *med17-670* and *-98*, respectively). In the *med17-670* mutant, a global 1.4-fold decrease in Pol II occupancy was observed when compared to the WT strain with the slope of regression line equal to 0.72 and a high correlation coefficient equal to 0.97. The Pol II association was also reduced in the *med17-98* mutant showing a 1.2-fold global decrease with a reduced correlation coefficient of 0.83 that suggested a more complex transcriptional effect for this mutation. The genome-wide analysis of PIC components of *med17-670* and *-98* mutants suggests that Mediator can selectively affect the TFIIH core subcomplex binding to the yeast genome without impairing that of the TFIIH kinase module or TBP.

DISCUSSION

In this study, a genome-wide analysis of PIC assembly *in vivo* was performed by taking advantage of conditional Mediator mutants of the essential Med17 head module subunit after a transfer to a non-permissive temperature. We propose that the Mediator head module in general, and Med17 in particular, independently coordinate the PIC assembly *in vivo* at different levels. (i) In accordance with previous studies, the results of this work support a central role for the Med17 Mediator subunit in Mediator organization and function. We demonstrate that *med17* mutants globally affect Pol II transcription and specific mutations in Med17 could result in a global destabilization of PIC assembly *in vivo*. (ii) The ChIP and ChIP-seq results show that Mediator selectively contributes to TBP recruitment or stabilization to chromatin *in vivo*, supporting Mediator head-TBP functional contact that was previously identified *in vitro*. (iii) We show that Mediator recruitment stabilizes TFIIK kinase and TFIIH core modules independently since *med17* mutations can differentially affect the genome-wide occupancy of the two TFIIH modules. We therefore propose that

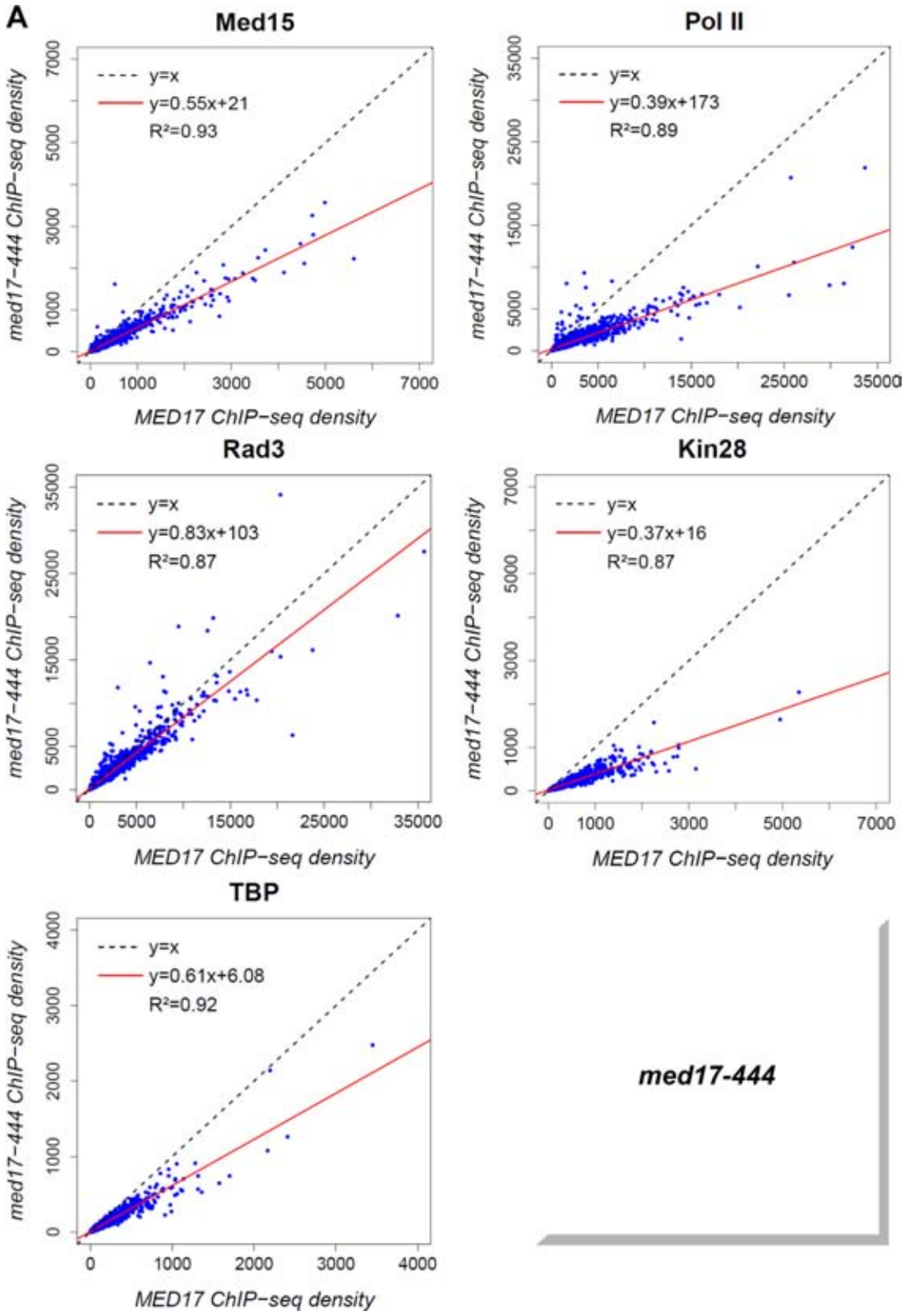
A
Med15
y=x
y=0.55x+21
R²=0.93
med17−444 ChIP−seq density
MED17 ChIP−seq density
Pol II
y=x
y=0.39x+173
R²=0.89
med17−444 ChIP−seq density
MED17 ChIP−seq density
Rad3
y=x
y=0.83x+103
R²=0.87
med17−444 ChIP−seq density
MED17 ChIP−seq density
Kin28
y=x
y=0.37x+16
R²=0.87
med17−444 ChIP−seq density
MED17 ChIP−seq density
TBP
y=x
y=0.61x+6.08
R²=0.92
med17−444 ChIP−seq density
MED17 ChIP−seq density
med17-444

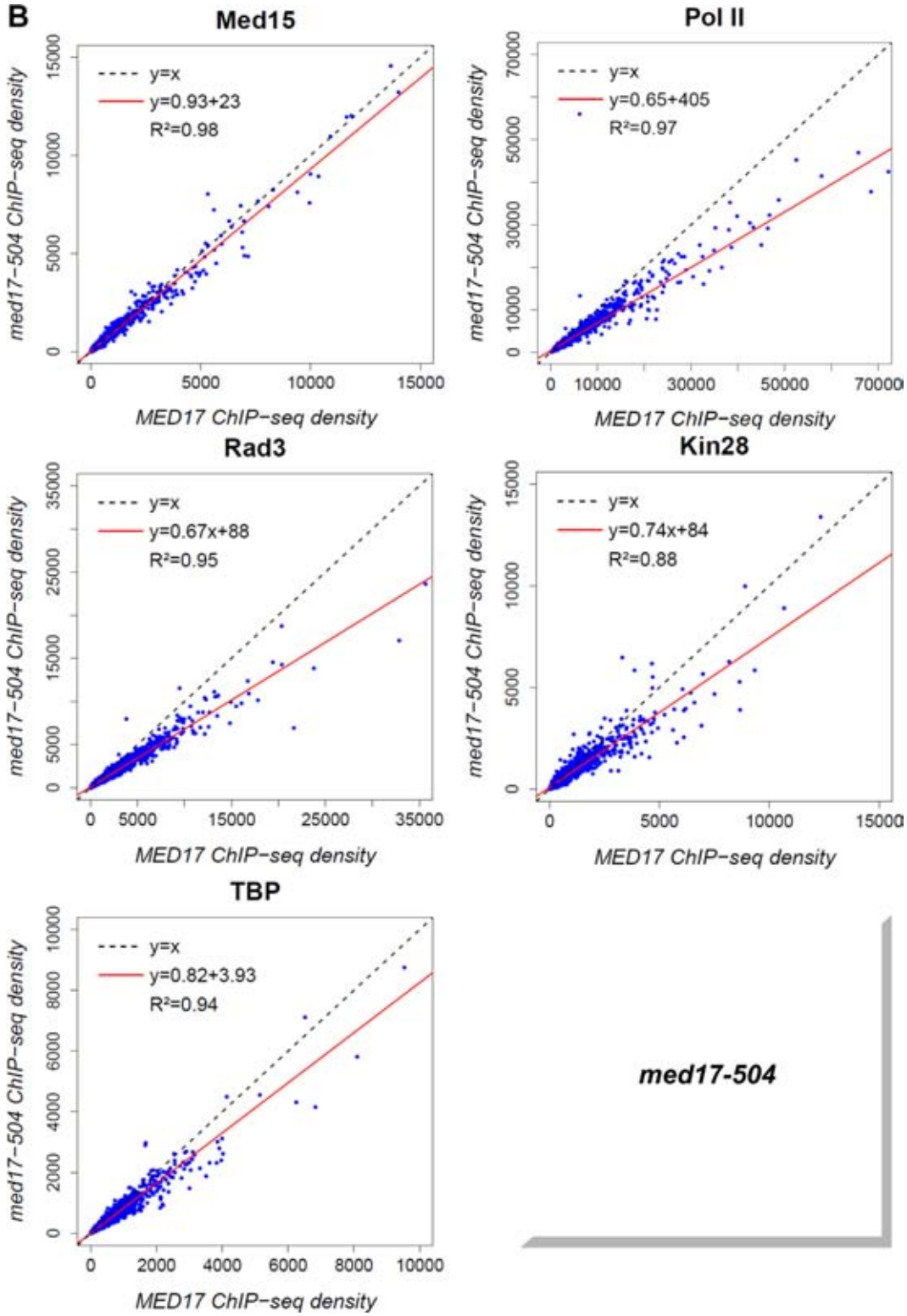

Figure 5. Global destabilization of PIC assembly in *med17-444 and -504* mutant strains. The density of sequence tags in Med15, Rad3, Kin28 and TBP ChIP-seq experiments was calculated for promoter regions of Pol II-transcribed genes. Cells were grown at 30°C in YPD medium and then transferred for 45 minutes to 37°C. The density of sequence tags in the Pol II ChIP-seq experiments was calculated for the Pol II-transcribed genes. In all, 3852 Pol II-enriched genes were used for these analyses. Tag densities were normalized relative to qPCR data on a set of selected genes. Each point on the plot corresponds to one promoter region or one ORF. Promoter regions correspond to intergenic regions in tandem or in divergent orientation, excluding intergenic regions encompassing Pol III-transcribed genes. A linear regression (red line) for ChIP-seq density in mutant versus ChIP-seq density in WT and an R^2 correlation coefficient are indicated. (**A**) Med15, Pol II, Rad3, Kin28 and TBP ChIP-seq density in *med17-444* versus ChIP-seq density in WT on class II promoter regions or ORFs (for Pol II). (**B**) Med15, Pol II, Rad3, Kin28 and TBP ChIPseq density in *med17-504* versus ChIP-seq density in WT on class II promoter regions or ORFs (for Pol II).

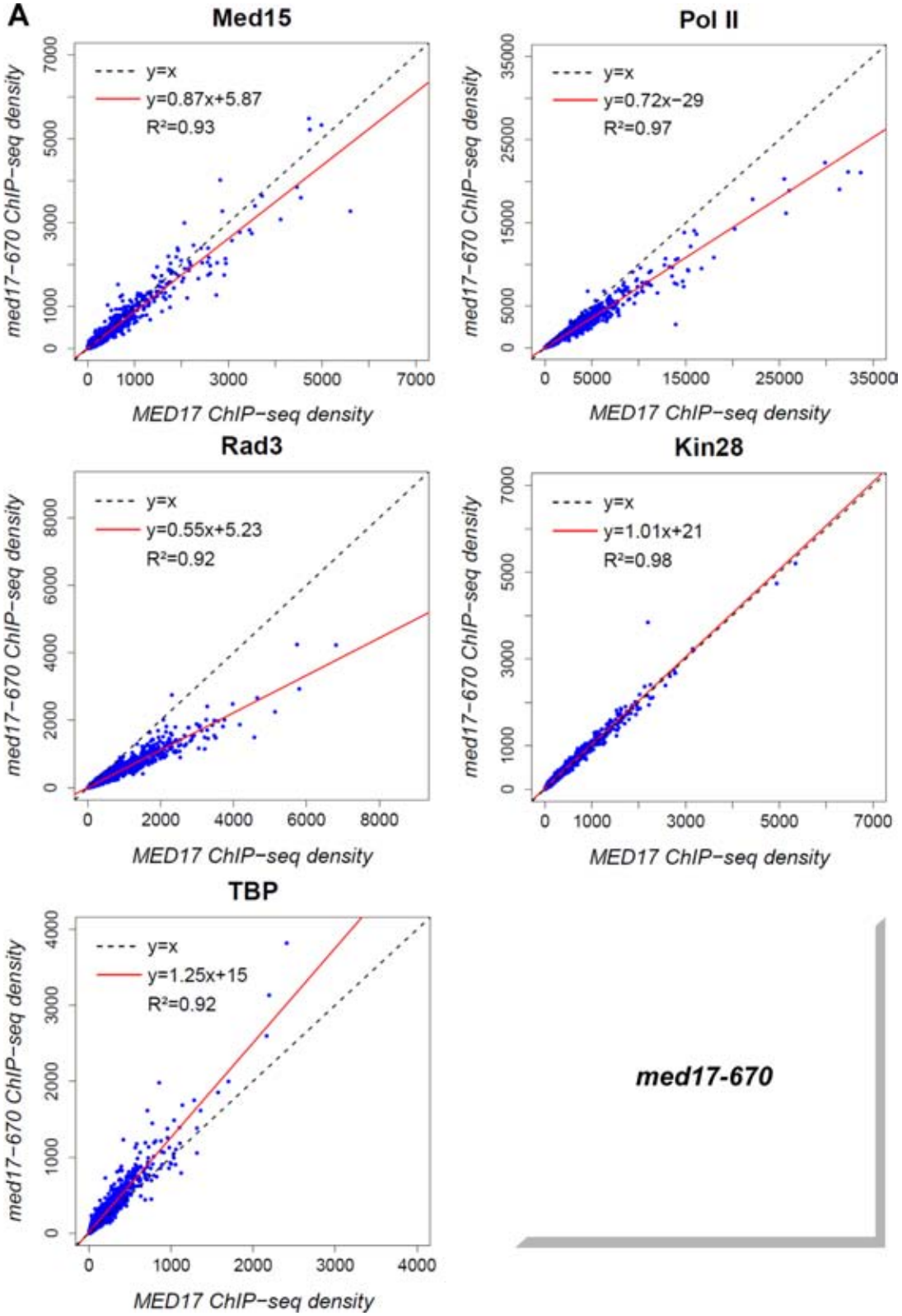
A
Med15
y=x
y=0.87x+5.87
R²=0.93
med17−670 ChIP−seq density
MED17 ChIP−seq density
Pol II
y=x
y=0.72x−29
R²=0.97
med17−670 ChIP−seq density
MED17 ChIP−seq density
Rad3
y=x
y=0.55x+5.23
R²=0.92
med17−670 ChIP−seq density
MED17 ChIP−seq density
Kin28
y=x
y=1.01x+21
R²=0.98
med17−670 ChIP−seq density
MED17 ChIP−seq density
TBP
y=x
y=1.25x+15
R²=0.92
med17−670 ChIP−seq density
MED17 ChIP−seq density
med17-670

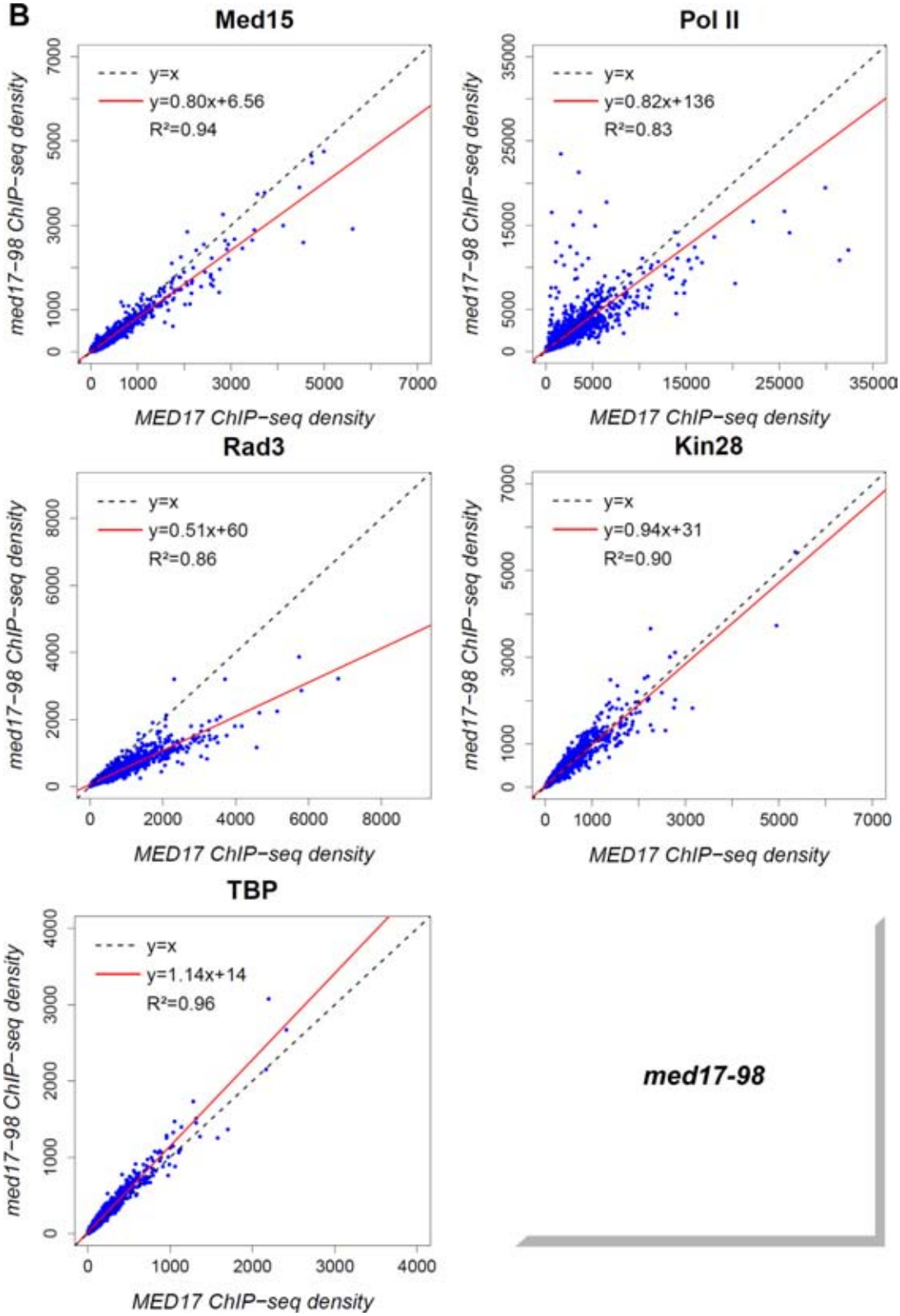

Figure 6. Global decrease of TFIIH core association independent of TFIIK in *med17-670 and -98* mutant strains. The density of sequence tags in the Med15, Pol II, Rad3, Kin28 and TBP ChIP-seq experiments was calculated as in Figure 5. (**A**) Med15, Pol II, Rad3, Kin28 and TBP ChIP-seq density in *med17-670* versus ChIP-seq density in WT on class II promoter regions or ORFs (for Pol II). (**B**) Med15, Pol II, Rad3, Kin28 and TBP ChIPseq density in *med17-98* versus ChIP-seq density in WT on class II promoter regions or ORFs (for Pol II).

the recruitment or the stability of TFIIH kinase and core modules is regulated independently on the yeast genome. (iv) This work suggests a possible mechanism for infantile cerebral atrophy caused by a mutation in Med17. We propose that the corresponding mutation in yeast Med17 affects Mediator–Pol II contact that leads to a global destabilization of PICs.

Independent recruitment of TFIIH modules

The Mediator head module directly interacts with the TFIIH complex via Med11-Rad3 contact and this interaction is important for the recruitment of this GTF to promoters (27). Mutations in the Med11 subunit differentially affected the promoter occupancy of the TFIIH core and TFIIK kinase modules. A *med11* mutation that impaired Mediator–TFIIH contact destabilized TFIIK on a group of promoters. The genome-wide analysis of *med17* mutants performed in this study supports a functional role of Mediator in the independent recruitment of TFIIH core (Rad3 subunit) and TFIIK kinase (Kin28 subunit) modules. Indeed, the *med17-504* mutation reduced the global association of Rad3 and Kin28 to a similar extent. On the contrary, the *med17-444* mutation, while affecting the occupancy of both TFIIH modules, displayed a particularly pronounced decrease in Kin28 occupancy. These results show that the TFIIK module was further destabilized in the *med17-444* mutant, similarly to the *med11-T47A* mutant. Conversely, we also observed that the genome-wide association of the TFIIH core subcomplex could be affected independently of the TFIIK subcomplex in *med17-670* and *med17-98* mutants. A large decrease of Rad3 genome-wide occupancy was observed in these mutants, whereas the association of the Kin28 TFIIK subunit remained unchanged. Taken together, these results suggest that Mediator differentially affects the recruitment or the stabilization of TFIIH modules and that the stability of TFIIH modules is regulated independently within the PICs. We show that two biochemically separable TFIIH modules have independent *in-vivo* behavior. The recruitment of the core TFIIH module can be selectively affected, independently of TFIIK and TBP. In line with the functional links between Mediator and TFIIK, one of the Mediator functions consists in stimulating the CTD phosphorylation by Kin28 TFIIK kinase (22). Moreover, Kin28 was reported to phosphorylate Med4 and Med14 Mediator subunits *in vitro* (60) and Kin28 phosphorylation of Med4 occurs *in vivo* (61). Recently, the phosphorylation of the Pol II CTD by Kin28 TFIIK kinase has been reported to regulate the transient association of Mediator to core promoters and a release of Mediator from the PIC and the promoter escape (15,56), highlighting reciprocal links between Mediator and the TFIIK kinase module.

Mediator contribution to TBP recruitment *in vivo*

TBP directly binds to the Mediator head module via the Med8–Med18–Med20 subcomplex (23,25). Previously, human Mediator and TBP-containing TFIID complexes have been shown to assemble cooperatively on promoter DNA *in vitro* (24). In accordance with *in-vitro* data, our *in-vivo* genome-wide analysis of yeast Mediator mutants showed that TBP chromatin binding could be affected by Mediator mutations (*med17-444* and *-504*). It should be noted that the loss of Mediator function in the *med17-138* mutant, in which the Mediator head disassembles, has been previously shown to reduce TBP occupancy of several class II promoters (62,63). TBP association depended on the Mediator mutant examined in this study. The genome-wide binding of this GTF either did not decrease or was found to slightly increase in the *med17-670* and *med17-98* mutants. In this work, we identified mutations in the Med17 subunit that affected global TBP binding to chromatin, further supporting a coordinated behavior with Mediator. Interestingly, even though the effects of *med17* mutations are global, the range of effects can depend on specific genes. For example, the *med17-504* mutation resulted in a global decrease in TBP occupancy, but did not affect TBP recruitment to the *GAL1* gene promoter upon transcription activation. Conversely, the *med17-98* mutation did not reduce genome-wide TBP or TFIIK occupancy. However, in this mutant the TFIIK binding, together with that of Pol II and the core TFIIH module, was reduced on the three model promoters, but not in the case of TBP. These results therefore suggest a selective contribution of Mediator in TBP recruitment or stabilization to chromatin.

Global stabilization of PIC by Mediator

In *med17-444* and *-504* mutants, PIC assembly was destabilized leading to a decrease of Pol II, Rad3 TFIIH core subunit, Kin28 TFIIK subunit and TBP presence. The following mechanistic explanations specific to each mutant can be proposed. The presence of the Mediator tail module (Med15 subunit) on chromatin was globally affected in the *med17-444* mutant. We propose that, as a consequence of this effect on tail module occupancy, overall PIC assembly is destabilized with a large decrease in Pol II, Kin28 and TBP occupancy and a moderate effect on Rad3 occupancy. In contrast, the binding of Mediator remained globally unaffected in the *med17-504* mutant. This mutation led also to a global decrease in Pol II and GTF occupancy. We propose that an impaired interaction between Mediator (the Med17 subunit) and Pol II (the Rpb3 subunit) in this mutant destabilized the global PIC assembly *in vivo*, as was observed for the Pol II *rpb3-2* mutant with reduced Mediator–Pol II interaction (28) highlighting the functional importance of Mediator–Pol II contact. Taken together, our results revealed that specific point mutations in the Med17 Mediator head subunit (*med17-Q444P*, *med17-M504P*) could result in the global destabilization of PIC assembly *in vivo* through two different mechanisms, a destabilization of Mediator binding to chromatin or an impaired interaction between Mediator and Pol II, consistent with a central role for the Med17 subunit in Mediator function.

Among the *med17* mutants examined, only the *med17-444* mutation reduced the global Mediator tail (Med15 subunit) occupancy. Other *med17* mutations either did not affect or only slightly reduced the level of genome-wide Med15 binding to chromatin. ChIP experiments on the *ADH1, PYK1* and *PMA1* genes did not reveal any decrease in Med6 Mediator head or Med5 Mediator tail subunit occupancy in *med17* mutants. Moreover, Mediator stability

in the *med17* mutants examined in this study is supported by mass spectrometry and CoIP experiments indicating the presence of all Mediator modules. A decrease in ChIP signal for the Med15 Mediator tail subunit in *med17-444* might reflect a conformational change in Mediator complex bound to chromatin leading to reduced cross-linking efficiency or Mediator tail destabilization on chromatin.

A possible mechanism for infantile cerebral atrophy

Mediator is conserved in all eukaryotes. The mutated residues in the *med17* mutants characterized in this study correspond to the same (human Q310 for yeast Q444P in *med17-444* and human E314 for yeast E448Q, one of the three mutations in *med17-98*) or functionally close (human L371 for yeast M504P in *med17-504*) amino acids in human Med17 protein (Supplementary Figure S6). Given the conservation of the Mediator subunits, the molecular mechanisms of the Mediator function in PIC assembly are probably conserved from yeast to human and might extend to all eukaryotes. We showed that the *med17-M504P* mutation, proposed to be equivalent to the human mutation responsible for infantile cerebral atrophy, led to a severe temperature-sensitive phenotype in yeast, impaired Pol II–Mediator interaction and resulted in a decrease of genome-wide occupancy of all PIC components tested except Mediator itself. These results suggest that infantile cerebral atrophy might be the direct consequence of a defect in Mediator–Pol II contact and a global destabilization of PICs. Recently, we have shown that Mediator, in addition to its coregulator role, can also serve as a link between transcription and DNA repair (45). Several *med17* mutants were UV-sensitive in a global-genome repair-deficient context. Furthermore, *med17–504* and the other mutants analyzed in this study do not show any increase in UV sensitivity (data not shown), suggesting that these mutations led to transcriptional defects only.

Specific versus global effects of *med17* mutations

One of the questions that we addressed in analysing the impact of conditional mutations in the Med17 Mediator subunit on genome-wide PIC assembly was its gene-specific versus global nature. A high correlation between genome-wide densities of PIC components highlights the global effects of *med17* mutations. It should be noted that the range of the effects could still be gene-specific. Consistent with a central role for the Med17 subunit in Mediator function, all *med17* mutations reduced the global Pol II chromatin binding, but to a varying extent. The global decrease of Pol II occupancy in *med17* mutants compared to the WT was associated with a high correlation coefficient, indicating that most of the genes were affected to a similar extent. The *med17-98* mutant was an exception since it showed a global decrease of Pol II presence but with a reduced correlation coefficient (R^2 equal to 0.83) suggesting a more complex and gene-specific transcriptional effect for this mutation. The occupancy of the Kin28 TFIIK subunit remained globally unchanged in the *med17-98* mutant compared to the WT, but Kin28 ChIP signals were decreased on the *ADH1, PYK1* and *PMA1* gene promoters. The *med17-444* mutation did not modify the presence of the Rad3 TFIIH core subunit on the three constitutively expressed genes or the *GAL1* inducible gene, but our genome-wide analysis revealed a slight decrease in global Rad3 occupancy. The *med17-504* mutant had a particular effect on the *GAL1* gene, showing a reduced Mediator association and unmodified Rad3 and TBP recruitment, whereas the genome-wide Mediator occupancy was similar to that of the WT and the occupancy of all other PIC components was globally reduced.

In conclusion, we suggest that Mediator differentially coordinates the multiple steps of a PIC assembly pathway *in vivo* at the level of independent recruitment or stabilization of several PIC components including Pol II, TBP and two TFIIH modules. The global effects of Mediator mutations on PIC formation are consistent with a central role for the Med17 subunit in Mediator function and organization. Additional PIC components, for example, GTFs that were not examined in this study, might contribute to PIC assembly. Together with Mediator, other coactivators, such as SAGA or TFIID complexes, modify PIC assembly and activity. In future studies it would be worth considering the dynamics of PIC assembly to improve understanding of *in-vivo* transcription mechanisms at work in eukaryotes.

SUPPLEMENTARY DATA

Supplementary Data are available at NAR Online.

ACKNOWLEDGEMENTS

We thank F.J. Asturias for CA001 strain, C. Thermes, E. Van Dijk and Y. Jaszczyszyn for performing the high throughput-sequencing of ChIP samples, the SPI (CEA/Saclay) for monoclonal antibodies and L. Kuras for critical reading of the manuscript. This work has benefited from the facilities and expertise of the high-throughput sequencing and the SICaPS mass spectrometry platforms of IMAGIF (Centre de Recherche de Gif, www.imagif.cnrs.fr).

FUNDING

Agence Nationale de la Recherche [ANR 11 BSV8 020 01, ANR-14-CE10-0012-01]; Fondation ARC [SL 2201130607079]; Fondation ARC [DOC20130606697 to F.E.]. Funding for open access charge: Fondation ARC [SL 2201130607079].
Conflict of interest statement. None declared.

REFERENCES

1. Buratowski,S., Hahn,S., Guarente,L. and Sharp,P.A. (1989) Five intermediate complexes in transcription initiation by RNA polymerase II. *Cell*, **56**, 549–561.
2. Ranish,J.A. and Hahn,S. (1996) Transcription: basal factors and activation. *Curr. Opin. Genet. Dev.*, **6**, 151–158.
3. Grunberg,S. and Hahn,S. (2013) Structural insights into transcription initiation by RNA polymerase II. *Trends Biochem. Sci.*, **38**, 603–611.
4. Rhee,H.S. and Pugh,B.F. (2012) Genome-wide structure and organization of eukaryotic pre-initiation complexes. *Nature*, **483**, 295–301.
5. Xu,Z., Wei,W., Gagneur,J., Perocchi,F., Clauder-Munster,S., Camblong,J., Guffanti,E., Stutz,F., Huber,W. and Steinmetz,L.M. (2009) Bidirectional promoters generate pervasive transcription in yeast. *Nature*, **457**, 1033–1037.

6. Tsai,K.L., Tomomori-Sato,C., Sato,S., Conaway,R.C., Conaway,J.W. and Asturias,F.J. (2014) Subunit architecture and functional modular rearrangements of the transcriptional mediator complex. *Cell*, **157**, 1430–1444.
7. Wang,X., Sun,Q., Ding,Z., Ji,J., Wang,J., Kong,X., Yang,J. and Cai,G. (2014) Redefining the modular organization of the core Mediator complex. *Cell Res.*, **24**, 796–808.
8. Guglielmi,B., van Berkum,N.L., Klapholz,B., Bijma,T., Boube,M., Boschiero,C., Bourbon,H.M., Holstege,F.C. and Werner,M. (2004) A high resolution protein interaction map of the yeast Mediator complex. *Nucleic Acids Res.*, **32**, 5379–5391.
9. Koschubs,T., Lorenzen,K., Baumli,S., Sandstrom,S., Heck,A.J. and Cramer,P. (2010) Preparation and topology of the Mediator middle module. *Nucleic Acids Res.*, **38**, 3186–3195.
10. Lariviere,L., Plaschka,C., Seizl,M., Wenzeck,L., Kurth,F. and Cramer,P. (2012) Structure of the Mediator head module. *Nature*, **492**, 448–451.
11. Robinson,P.J., Bushnell,D.A., Trnka,M.J., Burlingame,A.L. and Kornberg,R.D. (2012) Structure of the Mediator Head module bound to the carboxy-terminal domain of RNA polymerase II. *Proc. Natl. Acad. Sci. U.S.A.*, **109**, 17931–17935.
12. Kornberg,R.D. (2005) Mediator and the mechanism of transcriptional activation. *Trends Biochem. Sci.*, **30**, 235–239.
13. Ries,D. and Meisterernst,M. (2011) Control of gene transcription by Mediator in chromatin. *Semin. Cell Dev. Biol.*, **22**, 735–740.
14. Holstege,F.C., Jennings,E.G., Wyrick,J.J., Lee,T.I., Hengartner,C.J., Green,M.R., Golub,T.R., Lander,E.S. and Young,R.A. (1998) Dissecting the regulatory circuitry of a eukaryotic genome. *Cell*, **95**, 717–728.
15. Jeronimo,C. and Robert,F. (2014) Kin28 regulates the transient association of Mediator with core promoters. *Nat. Struct. Mol. Biol.*, **21**, 449–455.
16. Lacombe,T., Poh,S.L., Barbey,R. and Kuras,L. (2013) Mediator is an intrinsic component of the basal RNA polymerase II machinery in vivo. *Nucleic Acids Res.*, **41**, 9651–9662.
17. Paul,E., Zhu,Z.I., Landsman,D. and Morse,R.H. (2015) Genome-wide association of mediator and RNA polymerase II in wild-type and mediator mutant yeast. *Mol. Cell. Biol.*, **35**, 331–342.
18. Thompson,C.M. and Young,R.A. (1995) General requirement for RNA polymerase II holoenzymes in vivo. *Proc. Natl. Acad. Sci. U.S.A.*, **92**, 4587–4590.
19. Andrau,J.C., van de Pasch,L., Lijnzaad,P., Bijma,T., Koerkamp,M.G., van de Peppel,J., Werner,M. and Holstege,F.C. (2006) Genome-wide location of the coactivator mediator: Binding without activation and transient Cdk8 interaction on DNA. *Mol. Cell*, **22**, 179–192.
20. Zhu,X., Wiren,M., Sinha,I., Rasmussen,N.N., Linder,T., Holmberg,S., Ekwall,K. and Gustafsson,C.M. (2006) Genome-wide occupancy profile of mediator and the Srb8–11 module reveals interactions with coding regions. *Mol Cell*, **22**, 169–178.
21. Jiang,Y.W., Veschambre,P., Erdjument-Bromage,H., Tempst,P., Conaway,J.W., Conaway,R.C. and Kornberg,R.D. (1998) Mammalian mediator of transcriptional regulation and its possible role as an end-point of signal transduction pathways. *Proc. Natl. Acad. Sci. U.S.A.*, **95**, 8538–8543.
22. Kim,Y.J., Bjorklund,S., Li,Y., Sayre,M.H. and Kornberg,R.D. (1994) A multiprotein mediator of transcriptional activation and its interaction with the C-terminal repeat domain of RNA polymerase II. *Cell*, **77**, 599–608.
23. Cai,G., Imasaki,T., Yamada,K., Cardelli,F., Takagi,Y. and Asturias,F.J. (2010) Mediator head module structure and functional interactions. *Nat. Struct. Mol. Biol.*, **17**, 273–279.
24. Johnson,K.M., Wang,J., Smallwood,A., Arayata,C. and Carey,M. (2002) TFIID and human mediator coactivator complexes assemble cooperatively on promoter DNA. *Genes Dev.*, **16**, 1852–1863.
25. Lariviere,L., Geiger,S., Hoeppner,S., Rother,S., Strasser,K. and Cramer,P. (2006) Structure and TBP binding of the Mediator head subcomplex Med8-Med18-Med20. *Nat. Struct. Mol. Biol.*, **13**, 895–901.
26. Takahashi,H., Parmely,T.J., Sato,S., Tomomori-Sato,C., Banks,C.A., Kong,S.E., Szutorisz,H., Swanson,S.K., Martin-Brown,S., Washburn,M.P. *et al.* (2011) Human mediator subunit MED26 functions as a docking site for transcription elongation factors. *Cell*, **146**, 92–104.
27. Esnault,C., Ghavi-Helm,Y., Brun,S., Soutourina,J., Van Berkum,N., Boschiero,C., Holstege,F. and Werner,M. (2008) Mediator-dependent recruitment of TFIIH modules in preinitiation complex. *Mol. Cell*, **31**, 337–346.
28. Soutourina,J., Wydau,S., Ambroise,Y., Boschiero,C. and Werner,M. (2011) Direct interaction of RNA polymerase II and mediator required for transcription in vivo. *Science*, **331**, 1451–1454.
29. Bourbon,H.M. (2008) Comparative genomics supports a deep evolutionary origin for the large, four-module transcriptional mediator complex. *Nucleic Acids Res.*, **36**, 3993–4008.
30. Risheg,H., Graham,J.M. Jr, Clark,R.D., Rogers,R.C., Opitz,J.M., Moeschler,J.B., Peiffer,A.P., May,M., Joseph,S.M., Jones,J.R. *et al.* (2007) A recurrent mutation in MED12 leading to R961W causes Opitz-Kaveggia syndrome. *Nat. Genet.*, **39**, 451–453.
31. Schwartz,C.E., Tarpey,P.S., Lubs,H.A., Verloes,A., May,M.M., Risheg,H., Friez,M.J., Futreal,P.A., Edkins,S., Teague,J. *et al.* (2007) The original Lujan syndrome family has a novel missense mutation (p.N1007S) in the MED12 gene. *J. Med. Genet.*, **44**, 472–477.
32. Hashimoto,S., Boissel,S., Zarhrate,M., Rio,M., Munnich,A., Egly,J.M. and Colleaux,L. (2011) MED23 mutation links intellectual disability to dysregulation of immediate early gene expression. *Science*, **333**, 1161–1163.
33. Firestein,R., Bass,A.J., Kim,S.Y., Dunn,I.F., Silver,S.J., Guney,I., Freed,E., Ligon,A.H., Vena,N., Ogino,S. *et al.* (2008) CDK8 is a colorectal cancer oncogene that regulates beta-catenin activity. *Nature*, **455**, 547–551.
34. Gade,P., Singh,A.K., Roy,S.K., Reddy,S.P. and Kalvakolanu,D.V. (2009) Down-regulation of the transcriptional mediator subunit Med1 contributes to the loss of expression of metastasis-associated dapk1 in human cancers and cancer cells. *Int. J. Cancer*, **125**, 1566–1574.
35. Kuuselo,R., Savinainen,K., Sandstrom,S., Autio,R. and Kallioniemi,A. (2011) MED29, a component of the mediator complex, possesses both oncogenic and tumor suppressive characteristics in pancreatic cancer. *Int. J. Cancer.*, **129**, 2553–2565.
36. Li,L.H., He,J., Hua,D., Guo,Z.J. and Gao,Q. (2010) Lentivirus-mediated inhibition of Med19 suppresses growth of breast cancer cells in vitro. *Cancer Chemother. Pharmacol.*, **68**, 207–215.
37. Vijayvargia,R., May,M.S. and Fondell,J.D. (2007) A coregulatory role for the mediator complex in prostate cancer cell proliferation and gene expression. *Cancer Res.*, **67**, 4034–4041.
38. Zhang,X., Krutchinsky,A., Fukuda,A., Chen,W., Yamamura,S., Chait,B.T. and Roeder,R.G. (2005) MED1/TRAP220 exists predominantly in a TRAP/ Mediator subpopulation enriched in RNA polymerase II and is required for ER-mediated transcription. *Mol. Cell*, **19**, 89–100.
39. Thompson,C.M., Koleske,A.J., Chao,D.M. and Young,R.A. (1993) A multisubunit complex associated with the RNA polymerase II CTD and TATA-binding protein in yeast. *Cell*, **73**, 1361–1375.
40. Linder,T., Zhu,X., Baraznenok,V. and Gustafsson,C.M. (2006) The classical srb4–138 mutant allele causes dissociation of yeast Mediator. *Biochem. Biophys. Res. Commun.*, **349**, 948–953.
41. Takagi,Y., Calero,G., Komori,H., Brown,J.A., Ehrensberger,A.H., Hudmon,A., Asturias,F. and Kornberg,R.D. (2006) Head module control of mediator interactions. *Mol. Cell*, **23**, 355–364.
42. Takagi,Y. and Kornberg,R.D. (2006) Mediator as a general transcription factor. *J. Biol. Chem.*, **281**, 80–89.
43. Kaufmann,R., Straussberg,R., Mandel,H., Fattal-Valevski,A., Ben-Zeev,B., Naamati,A., Shaag,A., Zenvirt,S., Konen,O., Mimouni-Bloch,A. *et al.* (2010) Infantile cerebral and cerebellar atrophy is associated with a mutation in the MED17 subunit of the transcription preinitiation mediator complex. *Am. J. Hum. Genet.*, **87**, 667–670.
44. Ghavi-Helm,Y., Michaut,M., Acker,J., Aude,J.C., Thuriaux,P., Werner,M. and Soutourina,J. (2008) Genome-wide location analysis reveals a role of TFIIS in RNA polymerase III transcription. *Genes Dev.*, **22**, 1934–1947.
45. Eyboulet,F., Cibot,C., Eychenne,T., Neil,H., Alibert,O., Werner,M. and Soutourina,J. (2013) Mediator links transcription and DNA repair by facilitating Rad2/XPG recruitment. *Genes Dev.*, **27**, 2549–2562.
46. Soutourina,J., Bordas-Le Floch,V., Gendrel,G., Flores,A., Ducrot,C., Dumay-Odelot,H., Soularue,P., Navarro,F., Cairns,B.R., Lefebvre,O.

et al. (2006) Rsc4 connects the chromatin remodeler RSC to RNA polymerases. *Mol. Cell. Biol.*, **26**, 4920–4933.
47. Cai,G., Imasaki,T., Takagi,Y. and Asturias,F.J. (2009) Mediator structural conservation and implications for the regulation mechanism. *Structure*, **17**, 559–567.
48. Schmitt,M.E., Brown,T.A. and Trumpower,B.L. (1990) A rapid and simple method for preparation of RNA from Saccharomyces cerevisiae. *Nucleic Acids Res.*, **18**, 3091–3092.
49. Langmead,B., Trapnell,C., Pop,M. and Salzberg,S.L. (2009) Ultrafast and memory-efficient alignment of short DNA sequences to the human genome. *Genome Biol.*, **10**, R25.
50. Zhang,Y., Liu,T., Meyer,C.A., Eeckhoute,J., Johnson,D.S., Bernstein,B.E., Nusbaum,C., Myers,R.M., Brown,M., Li,W. *et al.* (2008) Model-based analysis of ChIP-Seq (MACS). *Genome Biol.*, **9**, R137.
51. Salmon-Divon,M., Dvinge,H., Tammoja,K. and Bertone,P. (2010) PeakAnalyzer: genome-wide annotation of chromatin binding and modification loci. *BMC Bioinformatics*, **11**, 415.
52. Spyrou,C., Stark,R., Lynch,A.G. and Tavare,S. (2009) BayesPeak: Bayesian analysis of ChIP-seq data. *BMC Bioinformatics*, **10**, 299.
53. Haimovich,G., Medina,D.A., Causse,S.Z., Garber,M., Millan-Zambrano,G., Barkai,O., Chavez,S., Perez-Ortin,J.E., Darzacq,X. and Choder,M. (2013) Gene expression is circular: factors for mRNA degradation also foster mRNA synthesis. *Cell*, **153**, 1000–1011.
54. Sun,M., Schwalb,B., Schulz,D., Pirkl,N., Etzold,S., Lariviere,L., Maier,K.C., Seizl,M., Tresch,A. and Cramer,P. (2012) Comparative dynamic transcriptome analysis (cDTA) reveals mutual feedback between mRNA synthesis and degradation. *Genome Res.*, **22**, 1350–1359.
55. Bonnet,J., Wang,C.Y., Baptista,T., Vincent,S.D., Hsiao,W.C., Stierle,M., Kao,C.F., Tora,L. and Devys,D. (2014) The SAGA coactivator complex acts on the whole transcribed genome and is required for RNA polymerase II transcription. *Genes Dev.*, **28**, 1999–2012.
56. Wong,K.H., Jin,Y. and Struhl,K. (2014) TFIIH Phosphorylation of the Pol II CTD Stimulates Mediator Dissociation from the Preinitiation Complex and Promoter Escape. *Mol. Cell*, **54**, 601–612.
57. Chen,Y., Negre,N., Li,Q., Mieczkowska,J.O., Slattery,M., Liu,T., Zhang,Y., Kim,T.K., He,H.H., Zieba,J. *et al.* (2012) Systematic evaluation of factors influencing ChIP-seq fidelity. *Nat. Methods*, **9**, 609–614.
58. Park,D., Lee,Y., Bhupindersingh,G. and Iyer,V.R. (2013) Widespread misinterpretable ChIP-seq bias in yeast. *PLoS One*, **8**, e83506.
59. Teytelman,L., Thurtle,D.M., Rine,J. and van Oudenaarden,A. (2013) Highly expressed loci are vulnerable to misleading ChIP localization of multiple unrelated proteins. *Proc. Natl. Acad. Sci. U.S.A.*, **110**, 18602–18607.
60. Liu,Y., Kung,C., Fishburn,J., Ansari,A.Z., Shokat,K.M. and Hahn,S. (2004) Two cyclin-dependent kinases promote RNA polymerase II transcription and formation of the scaffold complex. *Mol. Cell. Biol.*, **24**, 1721–1735.
61. Guidi,B.W., Bjornsdottir,G., Hopkins,D.C., Lacomis,L., Erdjument-Bromage,H., Tempst,P. and Myers,L.C. (2004) Mutual targeting of mediator and the TFIIH kinase Kin28. *J. Biol. Chem.*, **279**, 29114–29120.
62. Kuras,L. and Struhl,K. (1999) Binding of TBP to promoters in vivo is stimulated by activators and requires Pol II holoenzyme. *Nature*, **399**, 609–613.
63. Li,X.Y., Virbasius,A., Zhu,X. and Green,M.R. (1999) Enhancement of TBP binding by activators and general transcription factors. *Nature*, **399**, 605–609.